THE HELIUM WARM BREEZE IN IBEX OBSERVATIONS AS A RESULT OF CHARGE EXCHANGE COLLISIONS IN THE OUTER HELIOSHEATH

MACIEJ BZOWSKI, ¹ MARZENA A. KUBIAK, ¹ ANDRZEJ CZECHOWSKI, ¹ AND JOLANTA GRYGORCZUK ¹

¹Space Research Centre PAS (CBK PAN) Bartycka 18A 00-716 Warsaw, Poland

(Received July 1, 2016; Revised September 27, 2016; Accepted July 30, 2018)

Submitted to ApJ

ABSTRACT

We simulated the signal due to neutral He atoms, observed by Interstellar Boundary Explorer (IBEX), assuming that charge exchange collisions between neutral He atoms and He⁺ ions operate everywhere between the heliopause and a distant source region in the local interstellar cloud, where the neutral and charged components are in thermal equilibrium. We simulated several test cases of the plasma flow within the outer heliosheath and investigated the signal generation for plasma flows both in the absence and in the presence of the interstellar magnetic field. We found that a signal in the portion of IBEX data identified as due to the Warm Breeze does not arise when a homogeneous plasma flow in front of the heliopause is assumed, but it appears immediately when any reasonable disturbance in its flow due to the presence of the heliosphere is assumed. We obtained a good qualitative agreement between the data selected for comparison and the simulations for a model flow with the velocity vector of the unperturbed gas and the direction and intensity of magnetic field adopted from recent determinations. We conclude that direct-sampling observations of neutral He atoms at 1 AU from the Sun are a sensitive tool for investigating the flow of interstellar matter in the outer heliosheath, that the Warm Breeze is indeed the secondary population of interstellar helium, as it was hypothesized earlier, and that the WB signal is consistent with the heliosphere distorted from axial symmetry by the interstellar magnetic field.

Keywords: will be inserted later

Corresponding author: Maciej Bzowski

bzowski@cbk.waw.pl

1. INTRODUCTION

The Warm Breeze (WB) is a population of neutral He atoms that are flowing into the heliosphere in addition to the well-known population of pristine interstellar neutral (ISN) gas (Fahr 1968; Bertaux & Blamont 1971). The existence of WB was discovered by Bzowski et al. (2012) based on observations carried out using the IBEX-Lo neutral-atom detector (Fuselier et al. 2009) on board of the Interstellar Boundary Explorer (IBEX) space probe (McComas et al. 2009a). A reconnaissance study of the WB properties was presented by Kubiak et al. (2014). These latter authors suggested that WB is twice slower and twice warmer than the pristine ISN gas, it is coming from a direction different by $\sim 20^{\circ}$ to that of the ISN gas, and its density in front of the heliosphere is a few percent of that of ISN He. Both Bzowski et al. (2012) and Kubiak et al. (2014) considered a hypothesis that WB is the secondary population of interstellar neutral gas, similar to the secondary population of interstellar hydrogen, created in the outer heliosheath due to charge-exchange collisions between the unperturbed neutral population of interstellar matter and the heated, compressed, and deflected population of interstellar plasma in the outer heliosheath (OHS).

The existence of the secondary population of interstellar gas was suggested by Baranov & Malama (1993) for ISN H. This population, discovered indirectly in observations of the heliospheric backscatter glow in the Lyman- α line (Lallement & Bertaux 1990; Lallement et al. 1993), is produced in copious amounts in OHS due to the relatively high densities of the reaction substrates and the large reaction cross section (Lindsay & Stebbings 2005). The existence of a helium equivalent for the hydrogen secondary population can be expected as a result of several candidate charge exchange reactions (see Figure 24 and Table 2 in Bzowski et al. 2012). The most obvious candidate seemed to be:

$$H_{OHS} + He_{OHS}^+ \rightarrow He_{sec} + H_{OHS}^+,$$
 (1)

and it was considered by Müller & Zank (2003, 2004), who pointed out that the density of the secondary helium population expected in the heliosphere due to this reaction should be very low: about 1% of that of the primary ISN He. This was because of the very low reaction cross section for the collision speeds expected in the outer heliosheath (Barnett et al. 1990). However, Bzowski et al. (2012) pointed out that the most effective source of the secondary He is expected to be the charge exchange reaction between the He⁺ ions and He atoms:

$$\mathrm{He_{ISN}} + \mathrm{He_{OHS}^+} \rightarrow \mathrm{He_{sec}} + \mathrm{He_{OHS}^+}$$
 (2)

because even though the absolute densities of the He atoms and He⁺ ions in the outer heliosheath are an order of magnitude lower than these of H and H⁺, the reaction cross section is larger by a factor of 250.

Kubiak et al. (2016) analyzed data from observations by IBEX-Lo performed from 2009 to 2014 and determined the temperature, density and velocity vector of WB much more precisely than it was possible for Kubiak et al. (2014). In addition, at the time of the analysis by Kubiak et al. (2016) results of precise determination of the inflow direction of the unperturbed primary ISN He became available (Bzowski et al. 2014; Wood et al. 2015; Bzowski et al. 2015; Möbius et al. 2015; Schwadron et al. 2015; McComas et al. 2015a). Based on this insight, Kubiak et al. (2016) found that the inflow directions of ISN He, ISN H Lallement et al. (2005, 2010, available from), and WB are coplanar and that the plane in which these directions are included also includes the center of the IBEX Ribbon (McComas et al. (2009a); see also Funsten et al. (2013, 2015)). Later on, it was demonstrated that also the inflow direction of ISN O is within this plane (Schwadron et al. 2016) and that WB has its oxygen counterpart (Park et al. 2016). All this is a very strong evidence in favor of the hypothesis that WB is indeed the secondary population of ISN He.

This is because most of the state of the art heliospheric models, which treat the heliospheric and interstellar neutral populations kinetically (e.g., Izmodenov et al. 2005; Pogorelov et al. 2008), suggest that the direction of inflow of the heliospheric secondary population should be deflected from that of the primary population in the plane defined by the vectors of Sun's motion through the local interstellar medium and of the local interstellar magnetic field (ISMF). As a result of the action of ISMF, the heliosphere should be distorted from axial symmetry (Ratkiewicz et al. 1998), and the distribution of pressure, temperature, flow vectors of the plasma, and magnetic field intensity should be modified accordingly. The distortion predicted by purely-MHD models is mediated by the effects of charge-exchange between the plasma and ISN atoms (see also Izmodenov & Alexashov 2006; Izmodenov & Alexashov 2015; Pogorelov et al. 2006).

The direction of ISMF is expected to conform with the IBEX Ribbon direction, if the Ribbon is created via the secondary ENA emission mechanism (Heerikhuisen et al. 2010). This hypothesis is in agreement with in situ measurements of ISMF by Voyager (Burlaga & Ness 2014a,b) based as well on simple geometrical arguments (Grygorczuk et al. 2014) as on analysis performed using sophisticated heliospheric models (Zirnstein et al. 2016). In the secondary ENA emission mechanism, as suggested by McComas et al. (2009a) and Schwadron et al. (2009), the energetic neutral atoms (ENA) that are running radially away from the heliosphere are re-ionized beyond the heliopause and picked up by ISMF. They begin to gyrate around the field lines and eventually are re-neutralized due to charge exchange with atoms from the ambient ISN gas and run away in all directions, including those towards the Sun and the IBEX detectors. In the regions where the original ENA directions are close to perpendicular to the field lines, several scenarios (Heerikhuisen et al. 2010; McComas et al. 2009b; Schwadron et al. 2009; Chalov et al. 2010) have been proposed in which the signal observed by IBEX should be amplified with respect to the global ENA flux. Crucial in these scenarios is the geometry of the magnetic field. In all these scenarios, the source regions of the IBEX Ribbon is located close beyond the heliopause, its projection on the sky is close to circular, and the direction of ISMF is close to the center of this structure.

These scenarios, and especially that suggested by Heerikhuisen et al. (2010), gained credibility when Swaczyna et al. (2016a) determined parallax of the Ribbon and found that indeed, the Ribbon source is located at ~ 140 AU, i.e., beyond the distance to the heliopause found by Voyager 1 (Stone et al. 2013; Gurnett et al. 2013). Furthermore, Swaczyna et al. (2016b) were able to reproduce the dependence of the position of Ribbon center on ENA energy, discovered by Funsten et al. (2013, 2015). This was done using an analytic model adapted from Möbius et al. (2013), which assumes the secondary ENA emission mechanism due to Heerikhuisen et al. (2010), and adopting a spatial structure of the ENA emission from the supersonic solar wind resulting from observation-based solar wind structure, obtained by Sokół et al. (2015b).

These insights suggest a consistent physical scenario for the creation of the heliospheric boundary region, distorted from axial symmetry by the interstellar magnetic field, which forms due to interaction of the magnetized interstellar plasma with the latitudinally-structured solar wind and is mediated on one hand by the ISN gas, and on the other hand by the derivative charged populations of pickup ions, created in different regions inside and outside of the heliosphere, and by ENAs (for review, see Zank 2015). In this scenario, the plasma conditions in OHS, where the secondary ISN He is created, are strongly anisotropic, as illustrated by Heerikhuisen et al. (2014) and Izmodenov & Alexashov (2015), with relatively strong spatial gradients of the plasma velocity (both in magnitude and the flow direction), density, and temperature. Hence the local production rate of the secondary population must be strongly anisotropic, and since the neutral atoms move freely across the magnetic field lines, then effectively the distribution function of the secondary population of ISN He must be expected neither homogeneous, nor isotropic.

However, all these complexities were neglected by Kubiak et al. (2016) in their analysis of WB observations. These authors used a sophisticated method of data analysis and parameter fitting (Swaczyna et al. 2015) and a high-fidelity numerical scheme (Sokół et al. 2015a) to reproduce the data, but the physical model of WB they employed was, in fact, the so-called hot model of ISN gas, originally proposed by several authors in 1970s (e.g. Fahr 1978; Wu & Judge 1979). This model was modified to account for a variation in the ionization losses with time as proposed by Ruciński et al. (2003), and taking into account the most recent insight into the variation of the helium ionization rate (Bzowski et al. 2013; Sokół & Bzowski 2014; Sokół et al. 2016). However, the hot model assumes that the distribution function in the source region is given by the Maxwell-Boltzmann function with the parameters (bulk velocity, temperature, density) isotropic and homogeneous in space. Kubiak et al. (2016), as well as Kubiak et al. (2014) assumed that the distribution function of WB conforms to these prerequisites and that the source region is located at 150 AU from the Sun.

With these assumptions, using the sophisticated model of the measurement process executed by IBEX, they were able to successfully reproduce the observed signal and found the parameters of this model with surprisingly good precision (see the uncertainty discussion and data vs model comparison in Kubiak et al. 2016). While the χ^2 value they obtained statistically speaking is significantly too high, it is clear from inspection of the fit residuals shown by these authors that a large portion of this excess can be attributed to some residual non-He populations still present in the data. Generally, however, the model fits to data from all five IBEX observation seasons very well.

The high quality of data reproduction by the simple model used by Kubiak et al. (2016) is intriguing especially given one of the alternative hypotheses proposed by Kubiak et al. (2014) to explain WB, i.e., the hypothesis of a neutral He flow from a hypothetical nearby cloud-cloud interface. A mechanism potentially responsible for such a flow was proposed by Grzedzielski et al. (2010) for hydrogen. Kubiak et al. (2014) pointed out that for He it is even more plausible because due to a lower cross section for elastic scattering and a higher mass, He atoms will have a much larger path for thermalization, so the hypothetical cloud-cloud boundary layer may be located significantly farther away from the Sun than that needed in the original scenario proposed by Grzedzielski et al. (2010). The distribution function of such a flow would likely be relatively closely approximated by a Maxwell-Boltzmann distribution with a temperature higher than that of the ambient unperturbed ISN He, density much lower, and a different velocity relative to the Sun.

The objective of this paper is to verify the hypothesis that WB is indeed the secondary population of ISN He, created beyond the heliopause due to charge-exchange collisions between ISN He⁺ ions and ISN He atoms. To that end, we modify the simulation approach used by Kubiak et al. (2016) and we assume that the distribution function of ISN He is given by the isotropic Maxwell-Boltzmann function not at 150 AU, as adopted by Bzowski et al. (2015) and Kubiak et al. (2016), but much farther: at 5000 AU. With this, we adopt several simplified models of the plasma flow past the heliopause that have some of the features predicted by state of the art heliospheric models, and we allow for gains and losses of He atoms due to charge exchange along the trajectories of the ISN He atoms that actually reach the IBEX-Lo detector. We simulate (in a simplified way) the signal observed by IBEX-Lo in these different OHS models for several selected subsets of IBEX observations.

We demonstrate that under these assumptions the WB signal indeed is created and that it is sensitive to various aspects of the plasma in OHS, including the size of the OHS, its distortion from axial symmetry, the plasma temperature etc. We discuss the implications and suggest next steps in researching the interactions within and physical state of the interstellar matter in the boundary region of the heliosphere.

2. MODEL

2.1. The idea of the simulation

In this section we start with an outline of the idea of the simulation of the signal observed by IBEX-Lo used by Bzowski et al. (2015) and Kubiak et al. (2016) to simulate the ISN He and WB populations. Subsequently, we present the differences introduced to the model for the purpose of our study.

The signal simulation process used by these authors was presented in detail by Sokół et al. (2015a). Effectively, the signal (which is proportional to time-, energy-, and collimator-averaged differential flux) was calculated as an integral of the statistical weights $\omega_{\rm LOC}$ associated with a given ballistic trajectory of He atoms, determined by the location in space $\vec{r}_{\rm obs}$ of the detector and the heliocentric velocity vector $\vec{v}_{\rm obs}$ of the atom at $\vec{r}_{\rm obs}$. The atom velocity in the source region is $\vec{v}_{\rm src}$. The statistical weight $\omega_{\rm loc}$ was calculated as a product of the probability $f_{\rm src}(\vec{v}_{\rm src}(\vec{r}_{\rm obs},\vec{v}_{\rm obs}))$ that an atom at this trajectory exists in the source region and of the probability $w_{\rm ion}(\vec{r}_{\rm obs},\vec{v}_{\rm obs},r_{\rm src})$ that it is not ionized during its travel from the source region to the detection site at space $\vec{r}_{\rm obs}$:

$$\omega_{\text{loc}}(\vec{v}_{\text{obs}}) = f_{\text{src}}(\vec{v}_{\text{src}}) \, w_{\text{ion}}(\vec{r}_{\text{obs}}, \vec{v}_{\text{obs}}, r_{\text{src}}), \tag{3}$$

where $r_{\rm src}$ is the heliocentric distance of the source region. The relations between $\vec{v}_{\rm obs}$, $\vec{r}_{\rm obs}$ on one hand and $\vec{v}_{\rm src}$ on the other hand were obtained from solutions of the hyperbolic Kepler equation, obtained individually for all atoms, and the probabilities $w_{\rm ion}$ were calculated numerically along the trajectories taking into account the evolution of the ionization rate during the time needed to travel from the source region to the observation locus. The source distance $r_{\rm src}$ was fixed at 150 AU (for discussion of this choice, see McComas et al. 2015a), which is just outside the heliopause. Consequently, the assumption that there is virtually no production of He atoms between the source and detection loci was acceptable.

The local distribution function of ISN He at ~ 1 AU, where it is sampled by IBEX, is strongly anisotropic, as illustrated by Müller et al. (2016), and therefore must be integrated numerically. To obtain the simulated signal, the statistical weights $\omega_{\rm loc}$ were subsequently integrated over atom speeds relative to the detector and over the collimator transmission function $T_{\rm coll}$ to obtain the signal characteristic for a given line of sight. Since IBEX is a spinning spacecraft in an elongated orbit around the Earth, with the spin axis directed towards the Sun, the boresight of the IBEX-Lo instrument is continuously scanning a great circle in the sky. The spin period is divided into a fixed number of time intervals, which effectively correspond to fixed bins in the spin angle, which correspond to fixed regions in the sky. The IBEX spin axis is moved every few days to follow the Sun (once or twice per IBEX orbit), so at each orbit the instrument observes a different portion of the sky. To simulate this, the speed- and collimator-averaged flux was subsequently averaged over a selected spin angle bin $\Delta \psi$. Since the observations adopted for analysis are taken during several intervals of "good times" Δt_i , the simulated signal $F_{\rm sim}$ was further averaged over these time intervals. Effectively, the simulated signal for a given bin and a given orbit was calculated as:

$$F_{\text{sim}} = \frac{C \sum_{i} \int_{\Delta t_{i}} \int_{\Delta \psi} \int_{\Delta \Omega_{\text{coll}}} \int_{\Delta v_{\text{rel}}} T_{\text{coll}} v_{\text{rel}}^{3} \omega_{\text{loc}} dv_{\text{rel}} d\Omega_{\text{coll}} d\psi dt}{\sum_{i} \Delta t_{i}},$$
(4)

where C is a proportionality constant. All the necessary coordinate and reference system transformations are presented by Sokół et al. (2015a), who also discuss at length the important role of performing all of the above-mentioned integrations in obtaining a high-fidelity reproduction of the observed signal. A fundamental assumption in these calculations was that the parent distribution function at $r_{\rm src}$ is given by an isotropic

Maxwell-Boltzmann function $f_{\rm MB}$ co-moving with the ISN gas, which flows with the velocity $\vec{u}_{\rm LIC}$ relative to the Sun and has a temperature $T_{\rm LIC}$ and density $n_{\rm He,LIC}$, homogeneously distributed beyond the distance $r_{\rm src}$ from the Sun.

In the present approach, we set the source region of the observed atoms much farther away from the Sun, so far that the interstellar matter can be regarded as truly unaffected by any interaction with the solar output: $r_{\rm src}=5000$ AU. We follow a similar paradigm as outlined earlier, but now we allow for charge-exchange collisions to modify the statistical weights ω in the region outside the heliopause. For each of the test-particle atoms that reach our virtual detector, we now calculate ω as a result of a certain balance between the production and loss processes due to charge-exchange collisions between ISN He atoms and interstellar He⁺ ions:

$$\frac{d\omega}{dt} = \beta_{\text{prod}}(t) - \omega(t)\,\beta_{\text{loss}}(t),\tag{5}$$

where the solution is carried out along a given atom trajectory and β_{prod} , β_{loss} are the local instantaneous production and loss rates for the atoms following this trajectory. Since the atoms are following a Keplerian orbit, from conservation of angular momentum we can rewrite Equation (5) as a function of true anomaly θ of an atom on this trajectory. This requires a change of variables: $dt \to (r^2/L)d\theta$, where L is the magnitude of angular momentum per unit mass of the given atom.

As initial conditions for Equation (5) we demand that

$$\omega(\theta_{\rm src}) = \frac{n_{\rm He,LIC}}{\left(\pi \, u_{\rm T,LIC}^3\right)^{1/2}} \exp\left[-\left(\frac{\vec{v}_{\rm src} - \vec{u}_{\rm LIC}}{u_{\rm T,LIC}}\right)^2\right]. \tag{6}$$

Here, $\vec{v}_{\rm src}$ is the velocity vector of the given atom at the locus where its trajectory intersects the heliocentric distance $r_{\rm src}$. At this point, the true anomaly of this atom is $\theta_{\rm src}$. With this initial condition, we solve the production and loss balance Equation (5) until the trajectory intersects the heliopause. The heliopause location is adopted directly from the heliosphere model. There, we register the statistical weight $\omega_{\rm HP}$ and we restart atom tracking along its trajectory towards the detector in order to obtain its survival probability against ionization losses inside the HP $w_{\rm ion}$, exactly as it was done originally by Kubiak et al. (2016). Effectively, an analog to Equation (3) becomes:

$$\omega_{\text{LOC}}(\vec{r}_{\text{obs}}, \vec{v}_{\text{obs}}) = \omega_{\text{HP}} w_{\text{ion}};$$
 (7)

note that both $\omega_{\rm HP}$ and $w_{\rm ion}$ depend on $\vec{r}_{\rm obs}$ and $\vec{v}_{\rm obs}$.

In principle, the simulated signal could be calculated using Equation (4) taking into account all details of the measurement process and for all IBEX orbits for which observations of neutral He are available. In practice, however, solving for $\omega_{\rm HP}$ is a time-consuming numerical process and the problem becomes too demanding numerically. Therefore we simplify the simulation by calculating $F_{\rm sim}$ only for the middle time for several representative orbits; i.e., we do not perform averaging over good time intervals indicated in Equation (4). Further simplifications are not needed due to the way the Warsaw Test Particle Model (WTPM) simulation package operates. We estimate the numerical precision of the model at $\sim 1\%$.

The gist of the novelty in our paper is employing the charge-exchange interactions in Equation (5) to calculate a balance between the gains and losses of the He atoms reaching the detector. The production and loss terms for the He atoms following a given trajectory are calculated assuming various models of the plasma flow between the calculation boundary and the heliopause. In all of the models considered, we assume that the interstellar matter includes the primary, unperturbed population of ISN He, which is not

modified in any significant way in front of the heliopause and maintains its homogeneous velocity vector, temperature, and density. The interstellar matter includes a population of He⁺ ions which are in equilibrium with the local plasma flowing past the heliosphere. The flow is assumed to be invariable with time. In the following section we present details of the production and loss terms used in the calculation.

The assumption that the density, bulk velocity, and temperature of neutral helium, used to calculate the production and loss terms in Equation (5), does not vary in the calculation region outside of the heliopause is quite realistic. Charge exchange with He⁺ ions does not change the total number of neutral He atoms, and all He atoms in the region are potential candidates for charge exchange collisions, regardless of their collision history. Unlike in ISN H, modifications of the mean temperature and velocity of the total population of neutral He are very small because the absolute rate of charge exchange is small. The conclusion that the total He population very little differs from the unperturbed isothermal Maxwell-Boltzmann gas is supported by results of global heliospheric model with the helium charged and neutral populations taken into account self-consistently, shown in Figure 11 in Kubiak et al. (2014).

In our approach, we simulate the entire signal expected to be observed by IBEX without distinction what percentage of the simulated count rate in a given orbit and spin-angle bin is due to the pristine ISN He atoms that have not undergone any collision interactions, and which of the simulated counts are due to atoms produced by charge exchange collisions somewhere in front of the heliopause. Thus neither our simulation nor the observation is able to discriminate between atoms belonging to the primary and secondary populations.

This separation is not needed to compare the model with the observations. However, for illustration purposes, in some cases we will present the contribution of the secondary atoms to the simulated signal. This will be adopted as a difference between the simulated flux obtained for the given case (e.g., that presented in Section 3.3) and that obtained for the hot model scenario (Section 3.1).

The question of definition of the secondary population is only seemingly simple. In fact, however, this question is quite complex and different authors adopt different definitions. Osterbart & Fahr (1992), for example, defined the secondary, tertiary, and higher-order populations as those composed of atoms that participated in one, two, or more collisions within the calculation region. Müller et al. (2016) defined it as that due to any charge-exchange collisions within the perturbed region beyond the heliopause and modelled it as a separate fluid. But what exactly is the perturbed region sometimes is not clear, especially with kinetic models. For example, Zank et al. (2013) pointed out that when kinetic processes of interaction between the interstellar plasma and energetic neutral atoms emitted by the heliosphere are taken into account, then a region of increased plasma temperature extends far beyond the heliospheric bow wave or bow shock, and it is difficult to determine where exactly this heating effect vanishes. We alleviate all those dilemmas in our approach by adopting the working definition of the secondary component as specified in the preceding paragraph. If the calculation boundary is in a certainly undisturbed region, then calculating the target model and the reference hot model, and adopting the secondary population visible in the virtual collimator as the difference between these two is a well-defined and reasonable approach. The only differences between the solutions obtained from subtraction of the reference model from the target model can arise in the disturbedplasma region, regardless how far from this region is the calculation boundary located. If in a given scenario there is no perturbation beyond the bow shock, still our secondary population is only due to the perturbed region. If, on the other hand, there is no bow shock or a perturbation beyond the bow shock exists, our definition does not change and the secondary population from the entire affected region is taken into account.

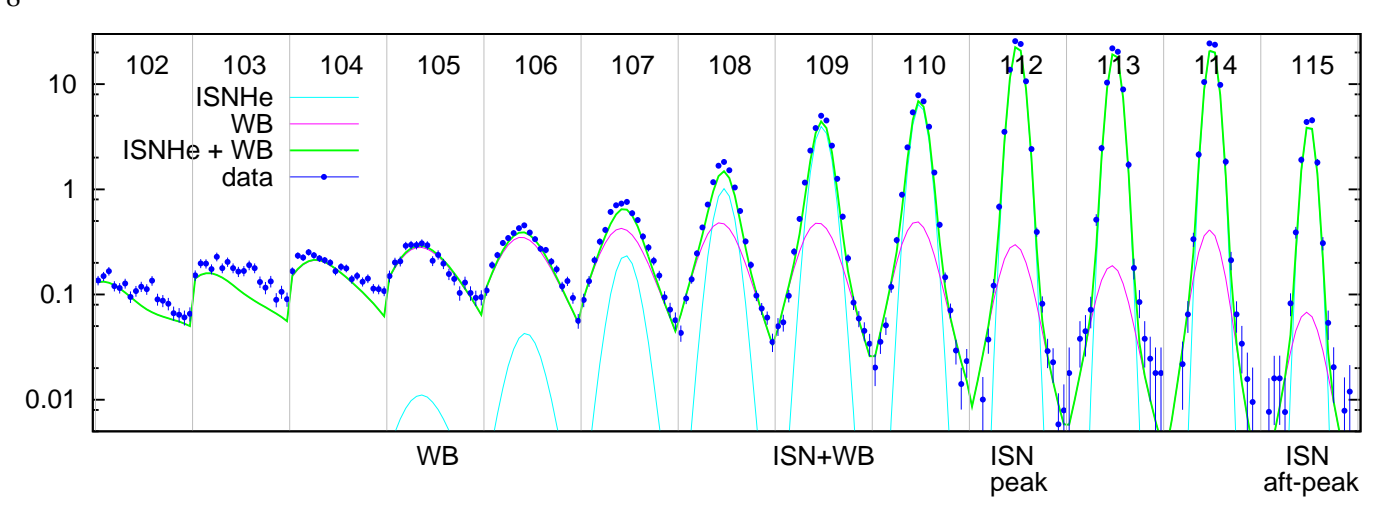


Figure 1. Illustration of the orbits selected for this analysis against data set from the entire ISN observation season 2011. Data from individual orbits are presented between vertical bars, and the orbit numbers are shown below the upper frame. Orbit-averaged count rates are shown as blue dots with error bars. Each of the blue dots corresponds to data from an individual spin-angle bin. The magenta and cyan solid lines illustrate the model signal for the WB and ISN He populations, respectively, calculated for the parameters of ISN He obtained by Bzowski et al. (2015) and those of WB obtained by Kubiak et al. (2016). In these calculations, all the details suggested by Sokół et al. (2015a) and Swaczyna et al. (2015) were taken into account and it was assumed that the parent populations for ISN He and WB are separate collisionless, homogeneous Maxwell-Boltzmann distribution functions. The green line is the sum of the simulated WB and ISN He signals; note that for some orbits practically the entire signal is due to WB. The orbits selected for our discussion: 105 (WB), 109 (ISN + WB), 112 (ISN peak), 115 (ISN aft-peak), are marked at the bottom of the upper panel.

As the production and loss processes we only admit the resonant charge-exchange collisions between He atoms and He⁺ ions. However, it will be clear from further discussion that additional gain and loss processes may be added (e.g., elastic collisions, electron-impact ionization, recombination, photoionization, charge exchange with H atoms and protons). The approximations acceptable for use in the calculation of charge-exchange reactions for heliospheric hydrogen and proton populations were recently discussed by Heerikhuisen et al. (2015). They point out that for distribution functions in the Maxwell-Boltzmann approximation and moderate temperatures it is sufficient to approximate the rate of charge exchange β_{AB} of a particle of type A traveling at some speed relative to a stationary Maxwell-Boltzmann population of particles B with a density $n_{\rm B}$, temperature $T_{\rm B}$, and particle mass $m_{\rm B}$ by the formula:

$$\beta_{AB} = n_B u_{rel,AB} \sigma_{cx}(u_{rel,AB}); u_{rel,AB} = u_{rel}(\vec{v}_A, \vec{u}_B, u_{T,B}), \tag{8}$$

where $u_{\rm rel,AB}$ is a certain effective relative speed between A and B. For this speed, we adopt:

$$u_{\rm rel,AB} = \left[\left(V_{\rm A} + \frac{1}{2V_{\rm A}} \right) \operatorname{erf}(V_{\rm A}) + \frac{\exp(-V_{\rm A}^2)}{\sqrt{\pi}} \right] u_{\rm T,B},\tag{9}$$

where $V_A = v_A/u_{T,B}$, and $u_{T,B} = (2k_B T_B/m_B)^{1/2}$ is the thermal speed of population B, $V_A u_{T,B}$ is the speed of particle A in the reference system co-moving with population B. The effective relative velocity $u_{rel,AB}$ is in fact a function of four parameters: the mean velocity of population A relative to Sun, the mean

¹ i.e., with mean velocity equal to 0.

velocity of population B relative to Sun, the thermal velocity of population B, and the specific velocity of a particle from population A with respect to its parent population. A formula for effective mean speed in this scenario was originally derived by Fahr & Mueller (1967) and repeated by Ripken & Fahr (1983). The formula we use, defined in Equation (9), was used by Fahr & Bzowski (2004) and is very similar to that used by Heerikhuisen et al. (2015). With this formula, for relative speeds of A much larger than the thermal speed of B ($V_A \gg 1$) the effective relative speed $u_{\rm rel} \to v_A$, and for $V_A \simeq 0$ the relative speed converges to the thermal speed: $u_{\rm rel} \to u_{\rm T,B}$.

We assumed that the charge exchange reaction defined in Equation (2) operates without momentum change between the reaction partners. For the charge exchange rate we need a formula that does not show an unrealistic behavior for very low reaction speeds (close to 0) and is valid up to $\sim 100 \text{ km s}^{-1}$. For this, we approximated a subset of data compiled by Barnett et al. (1990) by the following formula:

$$\sigma_{\rm cx}(u_{\rm rel}) = 3.752 \times 10^{-15} - 5.212 \times 10^{-16} \ln(u_{\rm rel}),$$
 (10)

where $u_{\rm rel}$ is the collision speed in km s⁻¹and $\sigma_{\rm cx}$ is in cm².

The production rate $\beta_{\mathrm{prod}}(t)$ is determined by the probability (given by the value of the distribution function $f_{\mathrm{He^+}}$ of the interstellar He⁺ ions) that a He⁺ ion with the velocity vector $\vec{v}(t)$ exists in the population of He⁺ ions at the location $\vec{r}(t)$ and that it enters into the c-x interaction with the ambient He population. This is reflected by the reaction cross section σ_{ex} multiplied by the relative speed of the collision partners. This rate is approximated by the formula:

$$\beta_{\text{prod}}(t) = n_{\text{He}} n_{\text{He}^+} f_{\text{He}^+}(\vec{v}, \vec{u}_{\text{He}^+}, u_{\text{T,He}^+}) u_{\text{rel}}^{\text{prod}} \sigma_{\text{cx}} \left(u_{\text{rel}}^{\text{prod}} \right);$$

$$u_{\text{rel}}^{\text{prod}} = u_{\text{rel}}(\vec{v}, \vec{u}_{\text{He}}, u_{\text{T,He}}), \tag{11}$$

where we keep in mind that the ISN He distribution is assumed to be homogeneous in space and its density, velocity, and temperature do not vary with \vec{r} . The loss rate per He atom is proportional to the entire local density of He⁺ ions because it is assumed that in the result of any c-x collisions the product He atom will have a different velocity vector from that before the collision. The loss rate per atom is then given by the formula:

$$\beta_{\text{loss}}(t) = n_{\text{He}^{+}} u_{\text{rel}}^{\text{loss}} \sigma_{\text{cx}} \left(u_{\text{rel}}^{\text{loss}} \right);$$

$$u_{\text{rel}}^{\text{loss}} = u_{\text{rel}}(\vec{v}, \vec{u}_{\text{He}^{+}}, u_{\text{T,He}^{+}}). \tag{12}$$

Note that the effective relative velocities $u_{\rm rel}^{\rm prod}$, $u_{\rm rel}^{\rm loss}$ in Equations (11) and (12) are different from each other.

2.3. IBEX orbit selection

Since on one hand our study has a qualitative character and on the other hand the amount of IBEX-Lo observations of neutral He is large, we believe it is not practical to simulate observations from all available orbits. Instead, we select four of them, characteristic for different aspects of the observed signal. We decided to choose data from the 2011 ISN observation season because during the first two seasons, 2009 and 2010, a considerable amount of ISN H was present in the data in addition to ISN He, which was reduced by a factor of 2 in the 2011 season (Saul et al. 2013). This was because due to an increase in solar activity in 2011, the solar radiation pressure increased and repelled most of ISN H atoms, preventing them from reaching the detector. Hence the counts observed in 2011 by IBEX-Lo were almost entirely due to He atoms, both for

the early orbits within the data set, where mostly WB is observed, and for the late, post-peak orbits, where Saul et al. (2012) and Saul et al. (2013) reported a considerable contribution from ISN H during the 2009 and 2010 ISN observation seasons.

The data from the 2011 ISN observation season are shown in Figure 1. For our study we chose four representative orbits that are well suited to study various aspects of the global signal. We selected the orbit where the observed signal due to the pristine ISN He is maximum, i.e., orbit 112; an orbit where Kubiak et al. (2016) suggested that only the WB signal is present, i.e., orbit 105; an orbit where the signal is due to both ISN He and WB in comparable proportions, i.e., orbit 109; and a late orbit during the season, where the signal is again almost entirely due to the ISN He population, and WB is expected to show up only far away from the signal peak, i.e., orbit 115. With this selection, we are able to study the symmetry of the simulated signal relative to the peak orbit depending on the adopted models of the ISN matter flow past the heliopause, to compare the intensity of the simulated signal with the data both for the peaks and in the far wings as a function of spin angle, and to study the buildup of WB in various scenarios.

2.4. Models of the interstellar matter in front of the heliopause

We performed simulations for several different scenarios for the interstellar matter in front of the heliopause, studying various aspects of the creation of the signal observed by IBEX-Lo. In all of the simulations, we assumed the densities of the neutral and charged H components in the unperturbed interstellar medium close to these obtained by Bzowski et al. (2008) and Bzowski et al. (2009) based on analysis of Ulysses pickup ion observations, and the temperature and bulk velocity of the unperturbed interstellar gas obtained by Bzowski et al. (2015) and Bzowski et al. (2014), Wood et al. (2015) based on direct-sampling observations on IBEX and GAS/Ulysses, respectively. The absolute density of ISN He far away from the Sun was adopted after Witte (2004) and Gloeckler et al. (2004), and the proportion between the neutral and two charged components of ISN He, used to calculate the absolute density of He⁺, after Slavin & Frisch (2008).

Note that in none of the adopted scenarios we assume preexistence of any population of neutral He in front of the heliosphere other than the unperturbed ISN He. All the differences in comparison with the classical hot model of ISN He are solely due to the action of charge exchange collisions between ISN He and interstellar He⁺ ions.

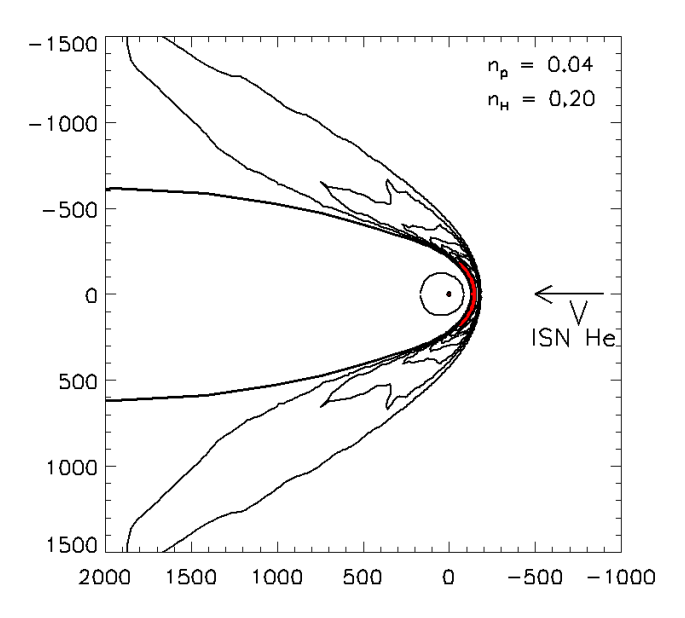
2.4.1. Hot model

We start from verifying the concept of the simulation and to that end we assume that the interstellar matter in front of the heliopause is not disturbed in any way by the presence of the heliosphere, i.e., that the plasma flow is homogeneous and isothermal. These assumptions are equivalent to the assumptions of the classical hot model of ISN gas distribution in the heliosphere, with the important exception that we allow for charge-exchange gains and losses in front of the heliopause.

In this scenario, we expect to reproduce the signal due to ISN He, but not that of the WB.

2.4.2. Bonn model

Subsequently, we do allow for modifications of the interstellar matter flow in the vicinity of the heliosphere but we neglect the interstellar magnetic field. In this case we can assume that the structure of the outer heliosheath is axisymmetric with respect to the inflow direction of the interstellar medium. For a detailed description we use the version of the Bonn model (Kausch & Fahr 1997), based on a numerical solution



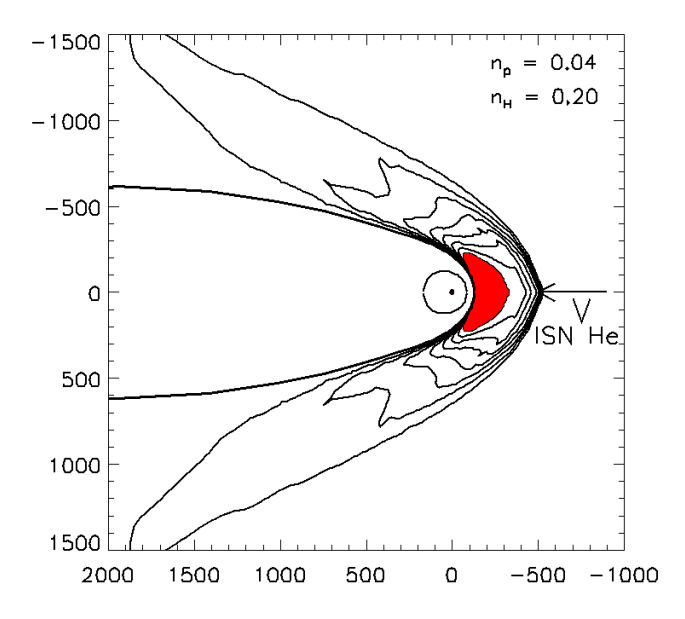


Figure 2. Plasma density contours obtained from the axially-symmetric, hydrodynamic model of the outer heliosheath by Kausch & Fahr (1997) (upper panel) and from the modified version of the model, with the region between the bow shock and the heliopause artificially expanded (lower panel).

of the hydrodynamical equations, with the inflow speed and temperature of the interstellar matter close to those obtained by Bzowski et al. (2015).

To calculate the Breeze production rates we need the parameters of the He⁺ component, which is not included explicitly in the Bonn model. We therefore assumed that the flow velocity and temperature of the He⁺ ion component in the OHS are equal to the corresponding parameters of the (mainly hydrogen) plasma

in the Bonn model, and that the He⁺ number density is a given constant fraction of 0.15 of the bulk plasma density. Figure 2 (top panel) shows the plasma density contours in the model.

We also considered a modified version of the model, in which spatial distributions of the parameters of the plasma and neutral components of the outer heliosheath were artificially expanded in distance, in order to increase the hot plasma region between the bow shock and the heliopause (Figure 2, bottom panel). The modified distributions F' are related to F of the original Bonn model by $F'(r',\theta) = F(r,\theta)$ and $r' - r_{HP}(\theta) = \alpha(\theta)(r - r_{HP}(\theta))$, where r is the heliocentric distance, θ the angle counted from symmetry axis, $r_{HP}(\theta)$ the distance to the heliopause, and $\alpha(\theta)$ the θ -dependent expansion factor. The modified model is no longer a solution of the hydrodynamical equations, but can be used to provide an approximate estimation of the effect of a wide hot plasma region in front of the heliopause. Effectively, this up-scaling results in a larger volume of the matter in front of the heliopause having an increased density and temperature.

In this scenario, we do expect some signal to appear in the IBEX orbit characteristic for WB (orbit 105) and we expect that the signal for the IBEX orbits where the primary ISN dominates to be modified due to the secondary population of He. In particular the heights of the peaks in orbits 109 and 115 will have different proportions to the height of the peak for orbit 112. Still, we expect systematic qualitative differences with the actual data because the flow past the heliopause in this scenario has axial symmetry around the inflow direction, which is not expected in reality due to the action of ISMF. By comparing two very similar models, differing only by the size of OHS, we can study the effect of the size of the OHS (equivalently, the "optical depth" for gains and losses) on the WB signal. An important aspect of this modified model is that the region of a higher density and temperature of the plasma is significantly larger than previously.

2.4.3. *MHD model*

Finally, we take into account the interstellar magnetic field, which breaks the axial symmetry of the interstellar flow past the heliopause, and we consider the role of plasma temperature. We use the results of the MHD simulations described in Grygorczuk et al. (2014) and Czechowski et al. (2015), for the particular case of interstellar field strength of 2 μ G. The velocity vector and temperature of ISN gas far away in front of the heliosphere are taken from McComas et al. (2015b) and the direction of the interstellar magnetic field towards the IBEX Ribbon center from Funsten et al. (2009). The MHD code used in our calculations is a corrected version of the one described by Ratkiewicz et al. (2008).

Our MHD model includes the interaction of plasma with the neutral component of the interstellar medium in a simplified form, in which the neutral flow is assumed to be constant, and there is no feedback from the plasma to ISN H. As a result of this simplification, the plasma temperature obtained tends to be lower than in global heliospheric models which take this feedback into account. Therefore, we consider two versions of the model: the MHD solution, and a modified version that differs from the MHD solution by the artificially increased temperature (multiplied by 2) in the region inside the isodensity contour 0.067 cm⁻³), which was chosen to define the boundary of the high plasma density region immediately outside the heliopause. The question of the temperature of the interstellar He⁺ component of the OHS plasma is not trivial anyway. As pointed out by Müller et al. (2016) in the context of creation of the secondary helium component, available literature emphasizes that charge exchange heats plasmas (Zank et al. 1996, 2013) and that the long equilibration time scales may result in the lack of equilibrium between the ions of different species in OHS (Zank et al. 2014).

Figure 3 shows the heliopause, termination shock, the color-coded temperature distribution inside the $0.067~\rm cm^{-3}$ plasma isodensity contour, and selected plasma flow lines in the B-V plane (the plane containing the Sun, the interstellar magnetic field and the interstellar matter velocity direction), which is the symmetry

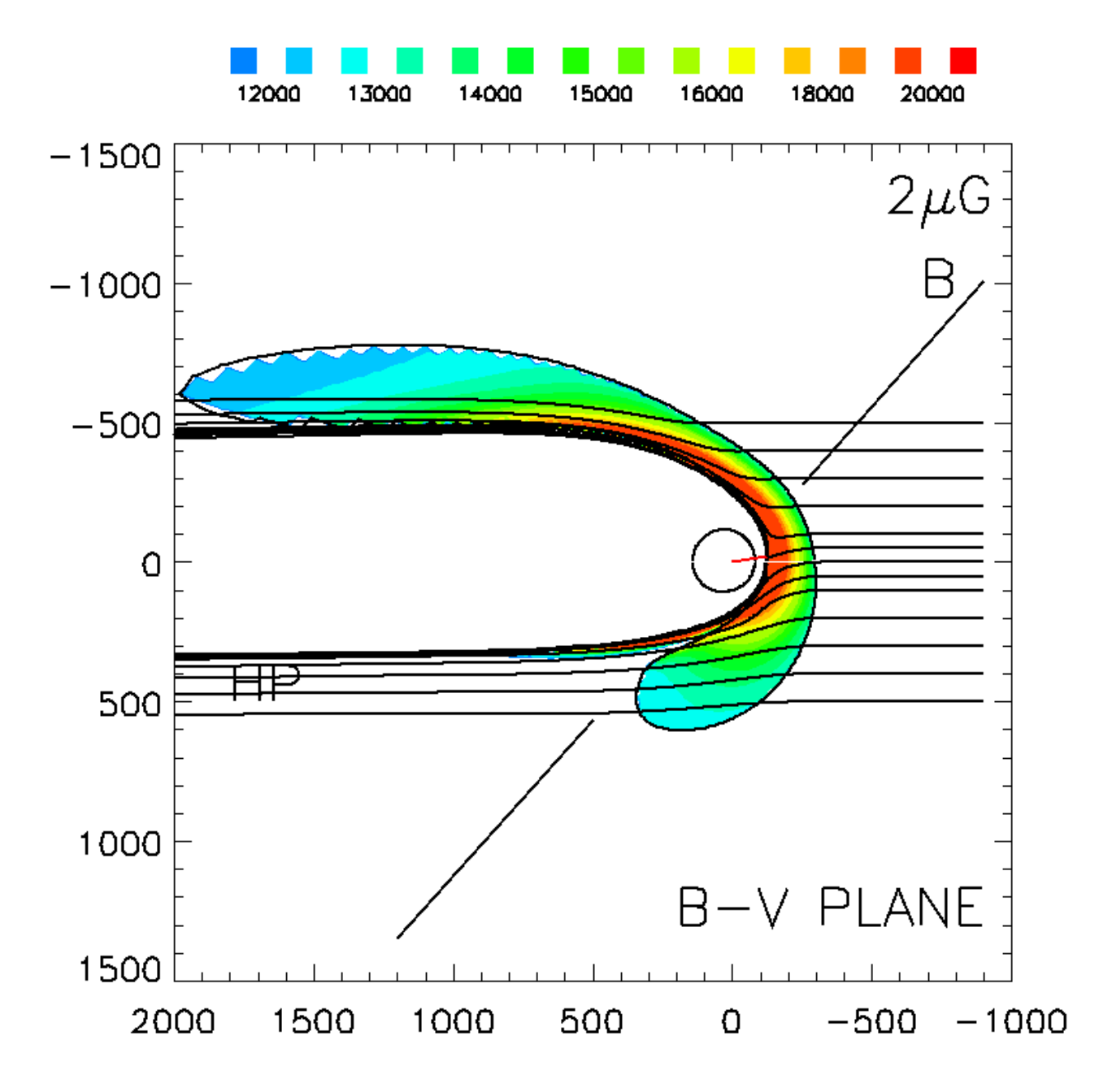


Figure 3. Color-coded distribution of plasma temperature within the region of enhanced plasma density outside the heliopause in the B-V plane (the plane containing the Sun, the interstellar magnetic field and the interstellar matter velocity direction). The temperature scale corresponds to the modified (rescaled) model. The unperturbed interstellar matter flows in from the right-hand side and its flow lines within the outer heliosheath are drawn with the black solid lines. The direction of the magnetic field is shown by the line denoted B. This direction was adopted towards the center of IBEX Ribbon. The small black oval centered at (0,0) is the termination shock. The inflow direction of WB found by Kubiak et al. (2016) is shown by the short red line extending from the Sun.

plane of the MHD solution. The B-V plane contains the inflow direction of WB found by Kubiak et al. (2016)), shown here by the short red line extending from the Sun. The temperature distribution color bar scale corresponds to the modified (doubled) values. The temperature for the nominal model can be read from the same figure with the scale values divided by two.

The helium component is not included explicitly in the MHD model. We obtain the density, velocity and temperature of the He⁺ ions based on the appropriate values of the simulated H⁺ plasma using the procedure described above for the Bonn model.

In this scenario, we may hope to see the features of the simulated signal close to the data because the OHS model has, at least approximately, the essential features expected in the reality, i.e., the decoupling of the plasma flow from the neutral gas flow, compression and heating of the plasma, and an asymmetry of the flow due to the action of ISMF. With two versions of the temperature, we can study the effect of the temperature on the WB signal.

3. RESULTS

3.1. Test case: the conditions characteristic for the classical hot model of ISN He in the heliosphere

Results of the simulation carried out assuming that both plasma and ISN gas are unperturbed everywhere beyond the heliopause, but that charge-exchange collisions operate outside the heliopause and contribute to the gains and losses of the He atoms following trajectories that hit the detector, are shown in Figure 4 (red line). The signal characteristic for the unperturbed ISN He population is reproduced well, and the signal attributed by Kubiak et al. (2016) as due to the Warm Breeze does not show up, in agreement with expectations. For the WB orbit (105) there is a very small signal predicted by both Kubiak et al. (2016) and the present model. Both of them, however, are below the background in the data, which for this orbit is at a level of $\sim 10^{-3}$ (Galli et al. 2015). For the orbits where ISN He dominates, WB is well visible at the wings of the central cores in the data and in the model by Kubiak et al. (2016) but not in the present simulations.

These results suggests that (1) the baseline concept of the simulation including the balance between the charge exchange gains and losses in the outer heliosphere is correct and our numerical code does not produce artefacts, and (2) indeed, charge exchange collisions in front of the heliosphere are not able to produce a signal due to He atoms in the region attributed to WB, when the plasma and gas in front of the heliosphere are unperturbed and thermalized with each other. In reality, the existence of these conditions is not expected.

3.2. Axially-symmetric flow in the absence of interstellar magnetic field (Bonn model)

Results of this simulation suggest that when the plasma flow in front of the heliopause is disturbed, a signal in the region characteristic for WB does appear. It is visible both in the pure-WB orbit 105 and in orbits 109 and 112 (as elevated wings), but not in the after-peak orbit 115, as illustrated in Figure 5, red line. However, the reproduction of the actually observed signal is not satisfactory even qualitatively. The maximum of the simulated signal for orbit 115 is too high by almost 30% and for orbit 109 too low by ~ 25 %. For the pure-WB orbit 105, the signal is too weak by an order of magnitude.

The quality of approximation given by the axially symmetric model is improved when the spatial extent of the OHS is artificially expanded, so that OHS extends to ~ 450 AU from the Sun, shown in the lower panel in Figure 2. The simulated signal is presented by black line in Figure 5. The wings of the signal are now elevated and they are qualitatively similar to the observed ones for orbits 109 and 112, and the signal is at a level well comparable to the observed one for the pure-WB orbit 105. However, the asymmetry in the peak heights between the orbits remains.

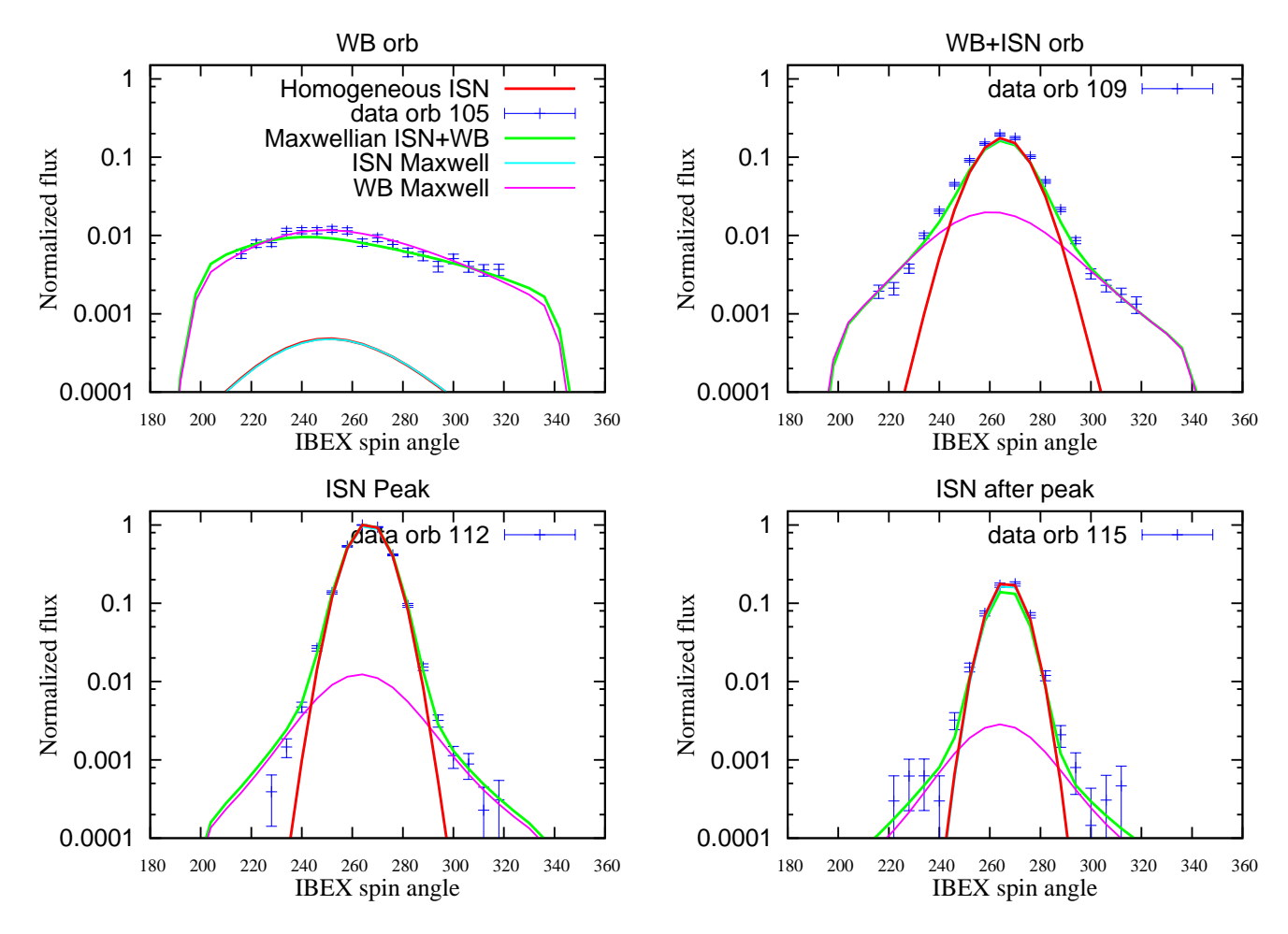


Figure 4. Comparison of (1) the data (blue dots), (2) model used by Kubiak et al. (2016), composed of the Maxwell-Boltzmann populations corresponding to ISN He (cyan) and WB (magenta), (3) the sum of the latter two (green), and (4) results of the present simulation for the homogeneous interstellar gas (red). The horizontal axis corresponds to the spin angle. Both the data and the models were normalized to their respective maximum values for orbit 112.

These results suggest that the intensity of the Warm Breeze signal is a function of the linear size of the outer heliosheath, as may be intuitively expected. Which of the parameters of the plasma is decisive in the reproduction of the observed signal: plasma density or temperature, will become evident in the next section. The systematic difference between the maxima of the model signal and that actually measured in the pre- and after-peak orbits suggests that axially symmetric heliospheric models are not likely to match the observed signal because the heliosphere is expected to be distorted due to interstellar magnetic field.

3.3. Asymmetric flow by the magnetized plasma (MHD model)

Results of simulating the neutral He signal observed by IBEX in the scenario with the ISMF included in the MHD model are presented in Figure 6 (red lines for the nominal case, black lines for the modified model with an increased temperature).

For the nominal MHD scenario, the signal for the WB orbit 105 fits qualitatively quite well to that observed. The heights of the signal peaks for the pre-peak and after-peak orbits 109 and 115 also agree very well with those observed (note that in this simulation we did not average the simulated flux over the good times, as it had been done by Kubiak et al. (2016)). This suggests that the distortion of the heliosphere by

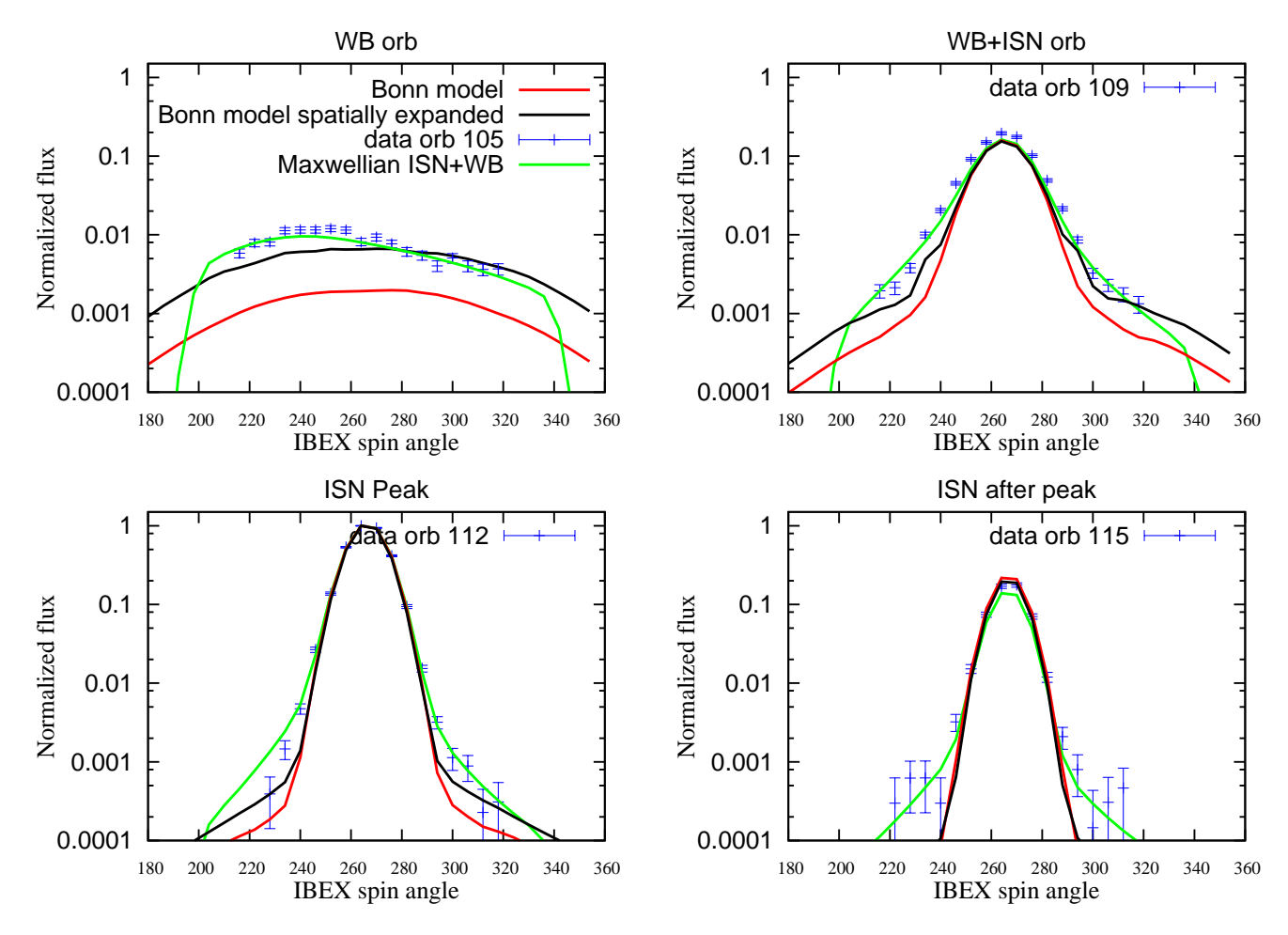


Figure 5. Comparison of (1) the data (blue dots), (2) model ISN + WB used by Kubiak et al. (2016) (green), (3) results of the present simulation with the plasma flow around the heliosphere according to the Bonn model (red; cf upper panel of Figure 2) and (4) results of the present simulation for the plasma flow from the re-scaled Bonn model (black; cf the lower panel of Figure 2). The horizontal axis corresponds to the spin angle. Both the data and the models were normalized to their respective maximum values for orbit 112.

the interstellar magnetic field with the direction and strength suggested by recent analysis carried out using state of the art models (Zirnstein et al. 2016) is needed to account for the signal from neutral He observed by IBEX. On the other hand, not all aspects of the actually observed signal were reproduced: the wings of the signal for all orbits except 105 were obtained too low.

For the modified MHD scenario, increasing the plasma temperature resulted in an increase of the simulated signal in the wings without affecting the peaks, so that now also this aspect is in a qualitative agreement with observations. This illustrates the sensitivity of the system to various aspects of the outer heliosheath, including its asymmetry of the flow due to magnetic field, spatial extent of the outer heliosheath, and particularly the temperature of plasma.

Ultimately, a simulation of the plasma flow in the OHS obtained from a relatively simple MHD model (with some temperature modifications) reproduced the signal due to neutral He observed by IBEX with a surprisingly good accuracy, at least for the selected representative subset of data. These simulations were carried out assuming the most up-to-date results for the direction and strength of LIMF and of the flow

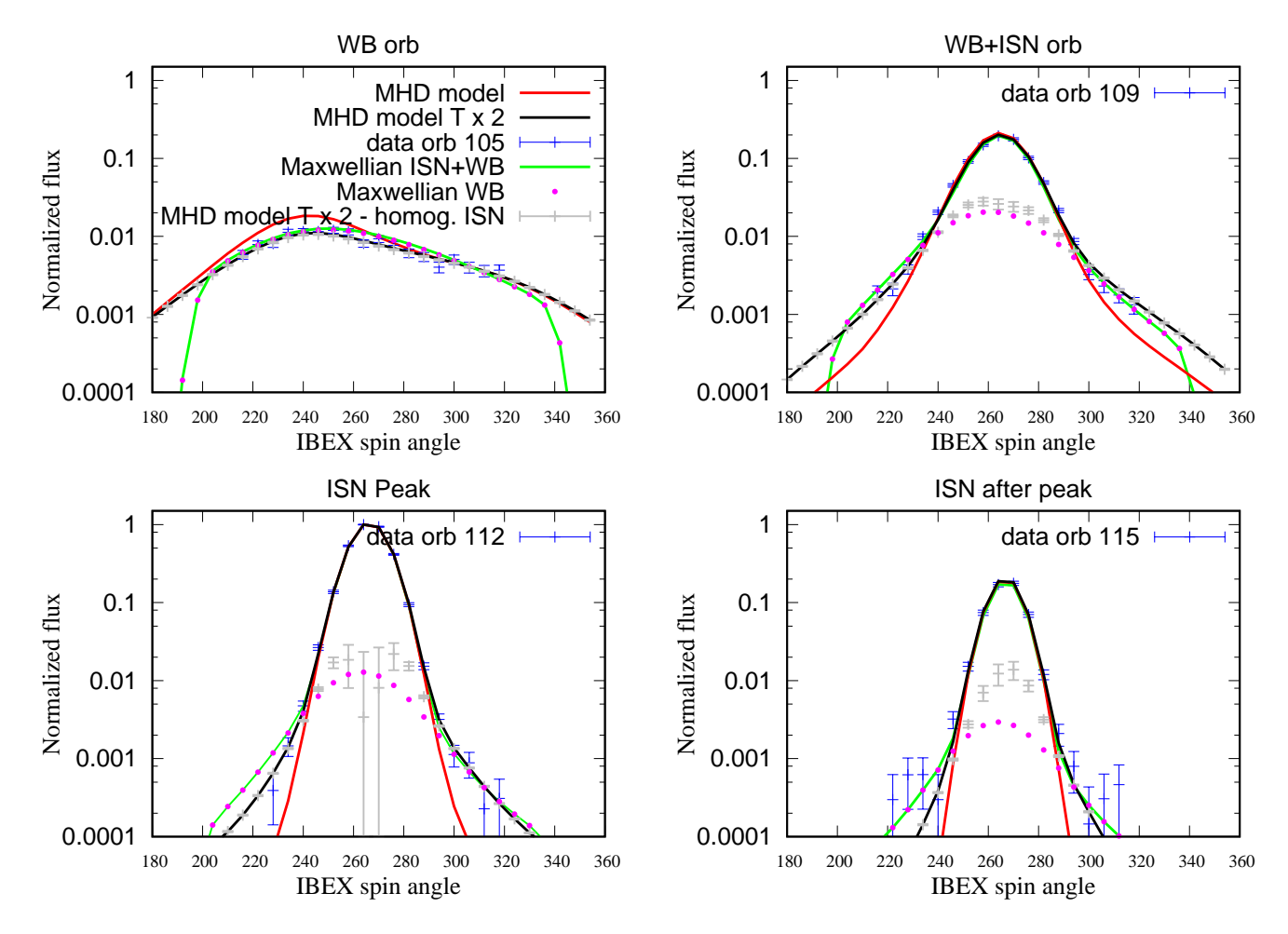


Figure 6. Comparison of the data (blue dots) with the ISN + WB model from Kubiak et al. (2016) (green) and simulation results for the MHD model of the outer heliosheath for interstellar magnetic field direction towards the center of IBEX Ribbon and an intensity of 2 μ G. Red lines mark the simulations performed for the nominal MHD model, black lines for the modified version of the model (Figure 3). Purple dots mark the Warm Breeze given by the Maxwell-Boltzmann population with the parameters found by Kubiak et al. (2016) and gray dots with error bars illustrate the difference between the modified MHD model (black line) and the hot model with no plasma modifications in front of the heliopause (the model drawn with red line in Figure 4). The error bars mark the numerical precision of the difference of the two models. The horizontal axis corresponds to the spin angle. Both the data and the models were normalized to their respective maximum values for orbit 112.

direction, velocity and temperature of interstellar gas in the LIC, and with the charge-exchange coupling between the He⁺ and He components of interstellar matter.

Keeping in mind the difficulty in formulating a clear definition of the secondary population in our approach, as discussed at the end of Section 2.1, we define the secondary population seen by IBEX as the difference between the flux simulated for a given test case and the flux simulated for the case with no plasma disturbance in front of the heliopause, discussed in Section 2.4.1 and shown in Figure 4. The secondary population signal thus defined is presented with the gray dots in Figure 6. For comparison, we additionally show the secondary population approximated by Kubiak et al. (2016) as due to a homogeneous Maxwell-Boltzmann flow outside the heliopause. Not surprisingly, in the pure-Warm Breeze orbit 112 the secondary population is responsible for practically entire signal, and for the pre-peak and peak orbits 109

and 112, respectively, it is close to the predictions given by the Maxwell-Boltzmann case. Note, however, that the numerical accuracy of our simulations, which is $\sim 1\%$, does not allow to separate the secondary population very accurately for the peak orbit 112. For the after-peak orbit 115, the model suggests the secondary population is much more plentiful close to the peak of the signal than in the two-Maxwellian case from Kubiak et al. (2016). We reiterate, however, that it is the agreement of the entire simulated signal with the data that is decisive to adopt or reject a given model.

3.4. In search for filtration of the primary ISN He population observed at 1 AU

Finally, we have assessed the hypothetical effect of filtration of the unperturbed ISN He population in the outer heliosheath. This effect was supposed by several authors (e.g. Möbius et al. 2015) to bias the ISN He parameters determined from direct-sampling observations of ISN He atoms, in particular the temperature of ISN He gas in front of the heliosphere. It was hypothesized that the beam of ISN He observed at ~ 1 AU from the Sun may be systematically narrowed to some extent as a function of spin angle, because some of the original interstellar atoms could be preferentially ionized in the outer heliosheath and thus eliminated from the observed sample. This effect could show up as a reduction of the width of the observed beam. Neglecting this hypothetical effect could lead to a biased estimate of the temperature of ISN He gas ahead of the heliosphere. This effect could be expected in analogy to the behavior of the primary and secondary populations of ISN H, suggested by Izmodenov et al. (2003a) and Izmodenov et al. (2003b) based on the Moscow MC model of the heliosphere.

With the simulations presented in this paper we are able to investigate at least qualitatively this hypothetical filtration effect. For comparison we took the results of the model where no plasma modification in OHS is considered on one hand (Figure 4), and on the other hand the model that fits best to the observations, i.e., the model with the ISMF intensity 2 μ G and the increased plasma temperature (Figure 6, black line). The first of these two models corresponds to the assumptions of the unperturbed hot model of ISN He in the heliosphere, similar to that used for analysis of the primary ISN He population by several authors (e.g., Witte 2004; Bzowski et al. 2012; Möbius et al. 2012; Bzowski et al. 2014, 2015; Leonard et al. 2015; Möbius et al. 2015; Schwadron et al. 2015). The other one represents a more realistic physical scenario, where the gains and losses due to charge exchange in OHS are taken into account. We compared the simulated flux for the peak and after-peak orbits, for which the WB is expected to be visible only in the far wings of the observed signal, and we took for analysis the spin angle range exactly as that used in the analysis of ISN He by Bzowski et al. (2015), i.e., $\psi \in (252^{\circ}, 288^{\circ})$. The simulated signals were fitted with a Gaussian function plus a constant background:

$$f(\psi) = bkg + f_0 \exp\left[-\left(\frac{\psi - \psi_0}{\sigma}\right)^2\right]$$
 (13)

and the values of σ obtained were $\sim 10.0^{\circ}$ for the peak orbit and $\sim 8.7^{\circ}$ for the after-peak orbit for the case of the classical hot model.

We found that consistently for both orbits considered, the σ parameter fit to the classical hot model was a little *lower* than that obtained for the model where the OHS c-x collisions were allowed for. These differences were very small in comparison with the σ value, 0.25° and 0.16° for the peak and after-peak orbits, respectively, i.e., about 2%. Therefore any expected systematic bias due to the neglected charge-exchange collisions operating in the OHS, affecting the temperatures found by the above-mentioned authors, is of a similar magnitude, i.e., negligible in comparison with the reported error margins. An interesting detail,

however, is that our simulations suggest that the small systematic effect is opposite to that hypothesized: instead of cooling the ISN He beam by differential ionization, some heating is observed, i.e., there is a net production of neutral He atoms observed in this interval of IBEX spin angles. This result indicates that the secondary component contributes to the entire signal observed by IBEX, including the pixels that in the original analysis of ISN He were treated as containing the pure ISN He gas. For the several pixels near the maximum count rate, this contribution is, however, very small and practically does not affect the width of the observed neutral helium beam.

3.5. Source regions for the He atoms observed by IBEX in different regions in the sky

A careful analysis of the ballistics of He atoms contributing to the total signal observed by IBEX at individual orbits showed that atoms registered in individual pixels enter the simulation region and cross the heliopause in well-defined strip-like regions, as illustrated in Figure 7. The atoms that define those regions are selected as those that contribute at least 0.001 of the total flux in a given pixels, but we verified that the regions practically do not change when one increases the cut-off level to 0.01 or 0.1. The overlap between the regions corresponding to individual pixels is approximately 20% of the widths of the strips. This overlap does not change with a change in the cut-off level. The exact location of the strips depends on one hand on the time of observation (the ecliptic longitude of the spacecraft), and on the other hand on the exact pointing of the spacecraft spin axis. However, the yearly pattern is approximately repeatable. The heliosphere entry regions for atoms contributing to the signal in a given pixel (spin angle bin) moves from orbit to orbit, but for a given orbit and a given pixel the entry region is definitely identifiable.

A similar observation was made by Kubiak et al. (2014) in the WB discovery paper, where the two Maxwell-Boltzmann populations model was used. The existence of the well-defined entry regions at the heliopause for atoms observed in individual spin angle bins is due to ballistics. Hence these regions are relatively robust against various assumptions on the processes operating in the OHS. Since most of the atoms follow approximately straight-line trajectories prior to entering the heliosphere, the regions identified in Figure 7 extend radially away without significant flexing at least for a few hundred AU from the heliopause. Thus the signal observed in individual pixels is an integrand over well-defined regions in the three-dimensional space outside the heliopause and this fact can be used to test various hypotheses on the behavior of matter in the OHS.

3.6. Outlook

The good qualitative agreement between the simulation results and the subset of observations we had chosen for comparison suggests that the methodology of simulating the expected signal has large diagnostic potential and may be used to discriminate between qualitatively different models of the heliosphere. Nowadays, three different models of the heliosphere are discussed in the literature: the canonical comet-like model, similar to that used in this paper (e.g., Izmodenov & Alexashov 2015; Heerikhuisen et al. 2014; Pogorelov et al. 2009), a croissant-like model due to Opher et al. (2015), or the diamagnetic bubble-like hypothesis due to Krimigis et al. (2009). A simulation of the expected signal of the secondary He population resulting from these models, calculated for any physical assumptions and values of the relevant parameters, can be done relatively easily based on a prediction of the plasma streamlines, density and temperature in a region in front of the heliopause.

Another logical step forward would be testing predictions of the current model against the entire data set available. This, however, requires optimizing the code to have it run faster. This work is underway now.

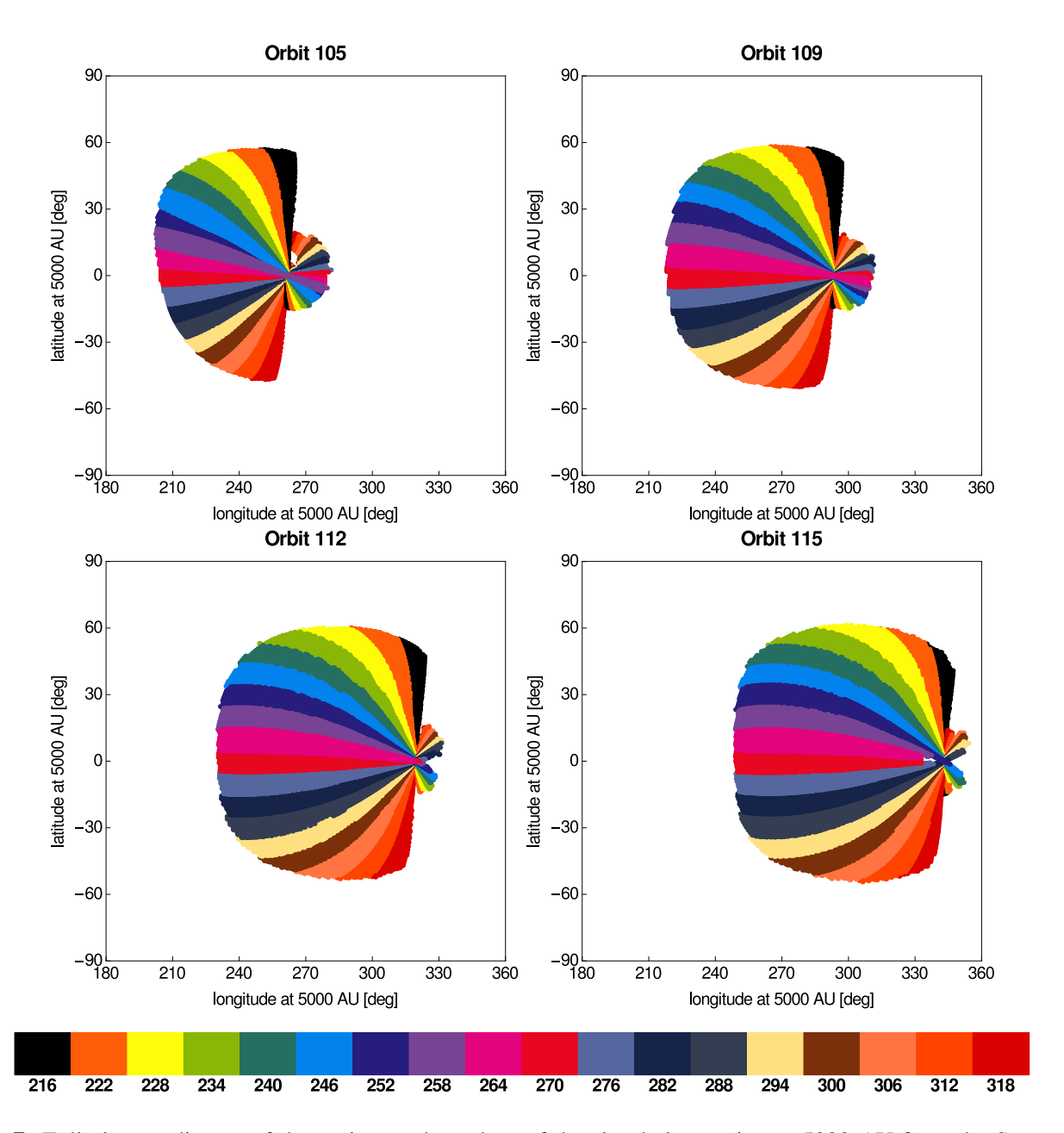


Figure 7. Ecliptic coordinates of the regions at boundary of the simulation region at 5000 AU from the Sun, where the atoms forming the signal observed by IBEX-Lo in individual pixels enter the calculation. The color code for spin angle bins (pixels) is given in the color bar. The spin angle bins correspond to the bins used to plot the simulated signal in Figure 6. The atoms used to determine these regions are those that contribute at least 0.001 of the calculated total flux in a given pixel.

4. SUMMARY AND CONCLUSIONS

The objective of this study was to verify if the WB signal observed by IBEX comes up naturally in the simulations when a physically reasonable model perturbation of the interstellar plasma flow due to the heliosphere's presence is adopted and charge-exchange collisions between He atoms and He⁺ atoms are assumed to operate. The positive outcome of this verification that we have obtained is another strong suggestion that WB is indeed the secondary population of ISN He, and that researching it may potentially

bring important insight into the physical state of interstellar matter in front of the heliopause and into processes operating in this region.

To accomplish this objective, we have extended the Warsaw Test Particle Model (WTPM) to account for gains and losses of ISN He atoms due to charge exchange in a region extending far away beyond the heliopause, and we simulated the signal expected to be observed by IBEX-Lo for several different models of the plasma flow beyond the heliopause. The purpose was not to precisely reproduce the observed signal, but to study the sensitivity of the signal to selected aspects of the plasma flow past the heliopause. We adopted the observation conditions characteristic for four carefully chosen IBEX orbits (Figure 1). In each of those orbits, a different aspect of the signal formation can be studied: pure WB, a mixture of WB and ISN He in comparable proportions, and orbits where ISN He dominates and WB is visible only in a subset of pixels. To add realism to our study, for numerical values of the density, bulk velocity, temperature, and ionization degree of the unperturbed gas we adopted those obtained from most up-to-date determinations, similarly as the direction and intensity of ISMF.

The most important conclusion from our study is that a simulated WB signal builds up naturally as soon as one allows for charge-exchange collisions operating within the plasma ahead of the heliopause, where the plasma flow is disturbed by the heliosphere. When this disturbance is absent, only the ISN He component is present in the simulated signal (Figure 4).

For an axially symmetric hydrodynamic model of the outer heliosheath, which predicts a relatively narrow sheath, the secondary population of ISN He would be visible for IBEX-Lo, but the simulated signal features important differences compared with the observations. Some of those differences, including an order of magnitude deficit in the pure-WB orbit, were partially removed by increasing the assumed size of the outer heliosheath. Other differences, including a strong deficit in the signal for the spin angle bins far away from the peak bins and the disturbed proportions between the signal peak heights among different orbits, remained (Figure 5).

For a MHD model with ISMF directed towards the IBEX Ribbon center and intensity in agreement with the current estimates, the resulting deformation of the heliosphere from axial symmetry removed the disagreement in the signal peak heights. Most of the remaining differences, especially in the wings of the signal, could be removed by increasing the plasma temperature inside the outer heliosheath. Furthermore, no up-scaling of the OHS size was required (Figure 6). This suggests that details of the temperature distribution of the plasma within OHS are more important for the creation of WB than the spatial extent of the OHS region.

These results suggest that even though the test models of the plasma flow we have used are not state of the art, apparently they are sufficiently realistic to grasp the most important features of the plasma flow beyond the heliopause. Details of the conditions in various regions of OHS can be studied in the future by detailed comparison of model results with observations. Due to the ballistics of ISN He atoms, the signal observed in individual pixels in the data from individual IBEX orbits can be mapped into distinct regions of OHS (Figure 7). Simultaneously, the portion of the observed signal corresponding mostly to the primary ISN He population does not seem to be morphologically biased by the secondary population and consequently the estimates of the temperature of the unperturbed local interstellar medium, obtained from analysis of direct sampling experiments, are not likely to be biased in an important way.

Results of the paper suggest that the classical, comet-like model of the heliosphere, traveling through a ~ 7500 K local interstellar medium at ~ 25 km s⁻¹ with a distortion due to ISMF of $\sim 2\mu$ G directed towards

the IBEX Ribbon center, is able to explain direct-sampling observations of interstellar neutral helium from IBEX.

Acknowledgment We thank Justyna Sokół for her help with the preparation of Figure 7. We are obliged to Romana Ratkiewicz for kindly providing us with an early version of the MHD code. This study was supported by Polish National Science Center grant 2015-19-B-ST9-01328.

REFERENCES

- Baranov, V. B., & Malama, Y. G. 1993, J. Geophys. Res., 98, 15157
- Barnett, C. F., Hunter, H. T., Kirkpatrick, M. I., et al. 1990, Atomic data for fusion. Collisions of H, H₂, He and Li atoms and ions with atoms and molecules, Vol. ORNL-6086/V1 (Oak Ridge, Tenn.: Oak Ridge National Laboratories)
- Bertaux, J. L., & Blamont, J. E. 1971, A&A, 11, 200Burlaga, L. F., & Ness, N. F. 2014a, ApJL, 795, L19—. 2014b, ApJ, 784, 146
- Bzowski, M., Kubiak, M. A., Hłond, M., et al. 2014, A&A, 569, A8
- Bzowski, M., Möbius, E., Tarnopolski, S., Izmodenov, V., & Gloeckler, G. 2008, A&A, 491, 7
- —. 2009, SSRv, 143, 177
- Bzowski, M., Sokół, J. M., Kubiak, M. A., & Kucharek, H. 2013, A&A, 557, A50
- Bzowski, M., Kubiak, M. A., Möbius, E., et al. 2012, ApJS, 198, 12
- Bzowski, M., Swaczyna, P., Kubiak, M., et al. 2015, ApJS, 220, 28
- Chalov, S. V., Alexashov, D. B., McComas, D., et al. 2010, ApJL, 716, L99
- Czechowski, A., Grygorczuk, J., & McComas, D. J. 2015, ArXiv e-prints, arXiv:1507.00540
- Fahr, H. J. 1968, Ap&SS, 2, 474
- —. 1978, A&A, 66, 103
- Fahr, H. J., & Bzowski, M. 2004, A&A, 424, 263
- Fahr, H. J., & Mueller, K. G. 1967, Z. Phys., 200, 343
- Funsten, H. O., Allegrini, F., Crew, G. B., et al. 2009, Science, 326, 964
- Funsten, H. O., DeMajistre, R., Frisch, P. C., et al. 2013, ApJ, 776, 30
- Funsten, H. O., Bzowski, M., Cai, D. M., et al. 2015, ApJ, 799, 68
- Fuselier, S. A., Bochsler, P., Chornay, D., et al. 2009, SSRv, 146, 117
- Galli, A., Wurz, P., Park, J., et al. 2015, ApJS, 220, 30 Gloeckler, G., Möbius, E., Geiss, J., et al. 2004, A&A, 426, 845

- Grygorczuk, J., Czechowski, A., & Grzedzielski, S. 2014, ApJL, 789, L43
- Grzedzielski, S., Bzowski, M., Czechowski, A., et al. 2010, ApJL, 715, L84
- Gurnett, D. A., Kurth, W. S., Burlaga, L. F., & Ness, N. F. 2013, Science, 341, 1489
- Heerikhuisen, J., Zirnstein, E., & Pogorelov, N. 2015, J. Geophys. Res., 120, 1516
- Heerikhuisen, J., Zirnstein, E. J., Funsten, H. O., Pogorelov, N. V., & Zank, G. P. 2014, ApJ, 784, 73
- Heerikhuisen, J., Pogorelov, N. V., Zank, G. P., et al. 2010, ApJL, 708, L126
- Izmodenov, V., Alexashov, D., & Myasnikov, A. 2005, A&A, 437, L35
- Izmodenov, V., Gloeckler, G., & Malama, Y. 2003a, Geophys. Res. Lett., 30, 3
- Izmodenov, V., Malama, Y. G., Gloeckler, G., & Geiss, J. 2003b, ApJL, 594, L59
- Izmodenov, V. V., & Alexashov, D. B. 2006, in AIP Conf. Proc. 858: Physics of the Inner Heliosheath, ed. J. Heerikhuisen, V. Florinski, G. P. Zank, & N. V. Pogorelov, 14–19
- Izmodenov, V. V., & Alexashov, D. B. 2015, ApJS, 220, 32
- Kausch, T., & Fahr, H. J. 1997, A&A, 325, 828
- Krimigis, S. M., Mitchell, D. G., Roelof, E. C., Hsieh, K. C., & McComas, D. J. 2009, Science, 326, 971
- Kubiak, M. A., Bzowski, M., Sokół, J. M., et al. 2014, ApJS, 213, 29
- Kubiak, M. A., Swaczyna, P., Bzowski, M., et al. 2016, ApJS, 223, 35
- Lallement, R., & Bertaux, J. L. 1990, A&A, 231, L3Lallement, R., Bertaux, J.-L., & Clarke, J. T. 1993,Science, 260, 1095
- Lallement, R., Quémerais, E., Bertaux, J. L., et al. 2005, Science, 307, 1447
- Lallement, R., Quémerais, E., Koutroumpa, D., et al. 2010, Twelfth International Solar Wind Conference, 1216, 555
- Leonard, T. W., Möbius, E., Bzowski, M., et al. 2015, ApJ, 804, 42

- Lindsay, B. G., & Stebbings, R. F. 2005,J. Geophys. Res., 110, A12213
- McComas, D., Bzowski, M. Fuselier, S., Frisch, P., et al. 2015a, ApJS, 220, 22
- McComas, D., Bzowski, M., Frisch, P., et al. 2015b, ApJ, 801, 28
- McComas, D. J., Allegrini, F., Bochsler, P., et al. 2009a, SSRv, 146, 11
- —. 2009b, Geophys. Res. Lett., 36, 12104
- Möbius, E., Liu, K., Funsten, H., Gary, S. P., & Winske, D. 2013, ApJ, 766, 129
- Möbius, E., Bochsler, P., Heirtzler, D., et al. 2012, ApJS, 198, 11
- Möbius, E., Bzowski, M., Fuselier, S. A., et al. 2015, ApJS, 220, 24
- Müller, H.-R., Möbius, E., & Wood, B. E. 2016, in Journal of Physics Conference Series, Vol. 767, Journal of Physics Conference Series, 012019
- Müller, H.-R., & Zank, G. P. 2003, in American Institute of Physics Conference Series, Vol. 679, Solar Wind Ten, ed. M. Velli, R. Bruno, F. Malara, & B. Bucci, 89–92
- Müller, H.-R., & Zank, G. P. 2004, J. Geophys. Res., 109, A07104
- Opher, M., Drake, J. F., Zieger, B., & Gombosi, T. I. 2015, ApJL, 800, L28
- Osterbart, R., & Fahr, H. J. 1992, A&A, 264, 260
- Park, J., Kucharek, H., Möbius, E., et al. 2016, ApJ, 833, 130
- Pogorelov, N. V., Heerikhuisen, J., & Zank, G. P. 2008, ApJL, 675, L41
- Pogorelov, N. V., Heerikhuisen, J., Zank, G. P., & Borovikov, S. N. 2009, SSRv, 143, 31
- Pogorelov, N. V., Zank, G. P., & Ogino, T. 2006, ApJ, 644, 1299
- Ratkiewicz, R., Barnes, A., Molvik, G. A., et al. 1998, A&A, 335, 363
- Ratkiewicz, R., Ben-Jaffel, L., & Grygorczuk, J. 2008, in Astronomical Society of the Pacific Conference Series, Vol. 385, Numerical Modeling of Space Plasma Flows, ed. N. V. Pogorelov, E. Audit, & G. P. Zank, 189–194
- Ripken, H. W., & Fahr, H. J. 1983, A&A, 122, 181Ruciński, D., Bzowski, M., & Fahr, H. J. 2003, Ann. Geophys., 21, 1315

- Saul, L., Wurz, P., Möbius, E., et al. 2012, ApJS, 198, 14
- Saul, L., Bzowski, M., Fuselier, S., et al. 2013, ApJ, 767, 130
- Schwadron, N., Möbius, E., Leonard, T., et al. 2015, ApJS, 220, 25
- Schwadron, N. A., Bzowski, M., Crew, G. B., et al. 2009, Science, 326, 966
- Schwadron, N. A., Möbius, E., McComas, D. J., et al. 2016, ApJ, 828, 81
- Slavin, J. D., & Frisch, P. C. 2008, A&A, 491, 53
- Sokół, J. M., & Bzowski, M. 2014, ArXiv e-prints, arXiv:1411.4826
- Sokół, J. M., Bzowski, M., Kubiak, M., & Möbius, E. 2016, MNRAS, 458, 3691
- Sokół, J. M., Kubiak, M., Bzowski, M., & Swaczyna, P. 2015a, ApJS, 220, 27
- Sokół, J. M., Swaczyna, P., Bzowski, M., & Tokumaru, M. 2015b, SoPh, 290, 2589
- Stone, E. C., Cummings, A. C., McDonald, F. B., et al. 2013, Science, 341, 150
- Swaczyna, P., Bzowski, M., Christian, E. R., et al. 2016a, ApJ, 823, 119
- Swaczyna, P., Bzowski, M., & Sokół, J. M. 2016b, ApJ, 827, 71
- Swaczyna, P., Bzowski, M., Kubiak, M., et al. 2015, ApJS, 220, 26
- Witte, M. 2004, A&A, 426, 835
- Wood, B. E., Müller, H.-R., & Witte, M. 2015, ApJ, 801, 62
- Wu, F. M., & Judge, D. L. 1979, ApJ, 231, 594
- Zank, G. P. 2015, ARA&A, 53, 449
- Zank, G. P., Heerikhuisen, J., Wood, B. E., et al. 2013, ApJ, 763, 20
- Zank, G. P., Hunana, P., Mostafavi, P., & Goldstein,M. L. 2014, ApJ, 797, 87
- Zank, G. P., Pauls, H. L., Williams, L. L., & Hall, D. 1996, J. Geophys. Res., 101, 21636
- Zirnstein, E. J., Heerikhuisen, J., Funsten, H. O., et al. 2016, ApJL, 818, L18